Dependence of electroporation detection threshold on cell radius: an explanation to observations non compatible with Schwan's equation model

Authors:

Borja Mercadal[1], P. Thomas Vernier[2] and Antoni Ivorra[1*]

Affiliations:

[1]Department of Information and Communication Technologies, Universitat Pompeu Fabra, Roc Boronat 138, Barcelona,08018, Spain

[2]Frank Reidy Research Center for Bioelectrics, 4211 Monarch Way, Norfolk, VA 23508, USA

Footnotes to the contribution title:

*Serra Húnter Fellow, Barcelona, Spain

Correspondence:

Antoni Ivorra

Department of Information and Communication Technologies, Universitat Pompeu Fabra, Roc Boronat 138, Barcelona,08018, SPAIN

Telephone number: (+34) 93 542 1578

Email address: antoni.ivorra@upf.edu

ABSTRACT

It is widely accepted that electroporation occurs when the cell transmembrane voltage induced by an external applied electric field reaches a threshold. Under this assumption, in order to trigger electroporation in a spherical cell, Schwan's equation leads to an inversely proportional relationship between the cell radius and the minimum magnitude of the applied electric field. And, indeed, several publications report experimental evidences of an inverse relationship between the cell size and the field required to achieve electroporation. However, this dependence is not always observed or is not as steep as predicted by Schwan's equation. The present numerical study attempts to explain these observations that do not fit Schwan's equation on the basis of the interplay between cell membrane conductivity, permeability and transmembrane voltage. For that, a single cell in suspension was modeled and it was determined the electric field necessary to achieve electroporation with a single pulse according to two effectiveness criteria: a specific permeabilization level, understood as the relative area occupied by the pores during the pulse, and a final intracellular concentration of a molecule due to uptake by diffusion after the pulse, during membrane resealing. The results indicate that plausible model parameters can lead to divergent dependencies of the electric field threshold on the cell radius. These divergent dependencies were obtained through both criteria and using two different permeabilization models. This suggests that the interplay between cell membrane conductivity, permeability and transmembrane voltage might be the cause of results which are non compatible with the Schwan's equation model.

KEYWORDS

Electroporation, Electropermeabilization, Cell size, Finite element modelling, Cell membrane,

Transmembrane transport, Membrane conductivity.

INTRODUCTION

Electroporation or electropermeabilization is a phenomenon in which the cell membrane, when exposed to short, high electric field pulses, increases its permeability to ions and macromolecules. This effect can be either transient or permanent depending on the magnitude of the field, the duration of the pulses, the number of pulses, and to a lesser extent, the pulse repetition frequency. Models for explaining the electroporation phenomenon (Chen et al., 2006) – which are supported by molecular dynamics simulations (Delemotte and Tarek, 2012; Ho et

al., 2013; Tarek, 2005; Ziegler and Vernier, 2008) – suggest that the observed increase in membrane permeability is initially due to the formation of hydrophilic pores in the lipid bilayer.

Exposure of a cell to an external electric field leads to an induced voltage across the cell membrane which is superimposed on the resting transmembrane voltage (TMV). Before electroporation occurs, this induced TMV can be quantified analytically for a spherical cell assuming a nearly insulating membrane by Schwan's equation (Kotnik and Miklavcic, 2000):

$$TMV = \frac{3}{2}|E_{ext}|R cos\theta \qquad (1)$$

where θ is the angle between the line defined from cell center to the evaluation point on the membrane and the applied external field (E_{ext}), and R is cell radius.

Although electroporation is not a bi-stable phenomenon, and cell membrane permeabilization exhibits a monotonically increasing dependence on the local TMV, this dependence is exponential (Glaser et al., 1988) and in practice so abrupt that it is widely accepted that electroporation occurs when the TMV reaches a certain threshold. This simplification is supported by experimental observations in which electroporation was noticed to behave as a threshold-like phenomenon (Abiror et al., 1979; Glaser et al., 1988; Kinosita et al., 1988; Melikov et al., 2001; Teissié and Rols, 1993; Zimmermann et al., 1974).

Under the threshold assumption, Schwan's equation leads to a proportionally inverse relationship (for a spherical cell) between the cell radius and the minimum magnitude of the applied electric field (E_c) for initiating electroporation.

$$E_c = \frac{2\ TMV}{3\ R\ cos\theta} \qquad (2)$$

There are, indeed, several published studies which report experimental evidences for an inverse relationship between the cell size and the electric field required to achieve electroporation (Agarwal et al., 2007; Mauroy et al., 2012; Sale and Hamilton, 1968; Sixou and Teissié, 1990; Tekle et al., 2001). However, this dependence is not always observed or is not as steep as predicted by Schwan's equation (Ĉemazâr et al., 1998; Henslee et al., 2011; Hojo et al., 2003; Ibey et al., 2011; Towhidi et al., 2008). We believe that these other results contradict the Schwan's equation model because that model is only valid for describing what happens just before electroporation of the poles of the cells facing the electrodes ($\theta = 0°, \theta = 180°$) and is no adequate for describing the conditions necessary to achieve detectable electroporation.

First, it must be noted that once the TMV reaches the critical value or threshold and electroporation takes place, membrane dielectric breakdown occurs in a few nanoseconds (Benz and Zimmermann, 1980; Frey et al., 2006;

1 Vernier et al., 2006; White et al., 2011) and membrane conductivity increases to a value that keeps the local

2 TMV of the electroporated regions of the cell close to its critical value. Increase in membrane conductivity tends

3 to reduce the TMV but if that happens then the conductivity decreases immediately and hence voltage goes up

4 again. This sort of negative feedback short-circuiting effect reduces the $\cos(\theta)$ dependence of local TMV in

5 Schwan's equation. The profile of the TMV along the membrane flattens at the poles facing the electrodes. This

6 was observed experimentally by Kinosita et al., (1988). Therefore, while Schwan's equation predicts a directly

7 proportional relationship between the applied field and the TMV over the whole cell, in reality a non-linear

8 relationship should be expected in which TMV increases at a lower rate once a field threshold is reached. In

9 other words, the Schwan's equation model overstates the TMV of an electroporated cell.

10 Secondly, it must be noted that assessment of electroporation is based on measurable effects such as dye uptake

11 (Golzio et al., 2002; Henslee et al., 2011; Sixou and Teissié, 1990), changes in membrane conductivity (Ivorra

12 and Rubinsky, 2007; Pavlin et al., 2005; Wegner, 2015), or cell lysis (Djuzenova et al., 1994; Ibey et al., 2011;

13 Sale and Hamilton, 1968) which are related to changes over a significant area of the membrane after

14 electroporation whereas the Schwan's equation model would only be intended to describe when electroporation

15 starts at an infinitesimal portion of the cell membrane area ($\theta = 0°, \theta = 180°$).

16 From these considerations we first hypothesized that, by modeling membrane conductivity changes during the

17 electroporation pulse, we might predict that in order to achieve a certain level of permeabilization the necessary

18 field (critical field) might not obey Schwan's equation model and might explain the apparently contradictory

19 experimental results regarding the dependence of electric field threshold on cell radius. We then extended the

20 study using a simple diffusion model to quantify the uptake of a probe solute after the electroporation pulse to

21 test the dependence of the critical field to achieve a certain intracellular concentration on the cell radius.

MATERIALS AND METHODS

23 In this study we defined two criteria to estimate the minimum electric field required to be able to detect

24 electroporation experimentally. The first criterion – related to changes that take place during the pulse – is that

25 we need to reach a minimum level of permeabilization during the pulse, characterized by the average relative

26 pore area (RPA) over the whole membrane. That is, we considered that electroporation occurs if the relative area

27 of the membrane occupied by pores reaches a threshold value (e.g. 0.01%).The second criterion – related to the

28 processes that take place after the electroporation pulse – is that we need to reach a certain intracellular

29 concentration of a specific ion or molecule after the application of the pulse.

Membrane permeabilization during the pulse

To model membrane permeabilization and conductivity changes during the pulse, we used and compared two different models. First, a membrane conductivity model (Ivorra et al., 2010) intended to reproduce the conductivity changes that would occur during the first microseconds after the pulse onset. Second, an electroporation model based on pore creation (DeBruin and Krassowska, 1999), to assess permeabilization and conductivity at the end of a typical electroporation pulse.

We numerically modeled electroporation of a single cell in a suspension using the finite element method (FEM) software platform COMSOL Multiphysics 4.4. The simulations were performed for both models, and according to the first criterion we defined we imposed values of the RPA. Then, for various values of cell radius, different magnitudes of the applied electric field were tested in the models in order to find the magnitude of the field that leads to the desired value of the RPA.

Model 1: Membrane conductivity model

A membrane conductivity model from Ivorra et al. (2010) – based on experimental measurements from Kinosita and Tsong (1979) – was used to describe membrane conductivity dependency on TMV in the first microseconds after the pulse onset due to the electroporation phenomenon:

$$\sigma_m = \sigma_{m0} + K(e^{\beta|TMV|} - 1) \tag{3}$$

where σ_{m0} is the conductivity of the membrane at the resting TMV and K and β are two constants adjusted to fit experimental measurements. If we assume that the membrane conductivity increase is due to the creation of pores, Eq. 3 can be written as:

$$\sigma_m = \sigma_{m0} + \sigma_p \left(\lambda \left(e^{\beta|TMV|} - 1 \right) \right) \tag{4}$$

where λ would be another constant, and σ_p is the equivalent conductivity of the medium filling the pores. The term $\lambda \left(e^{\beta|TMV|} - 1 \right)$ would represent the local relative pore area, and therefore the constant K on Eq. 3 depends on σ_p.

The steady state problem for the geometry depicted in **¡Error! No se encuentra el origen de la referencia.** was solved in the *Electric currents* mode of the *AC/DC* module of COMSOL (*Stationary Study*) using the linear system solver *Pardiso*. The conductivities of the intracellular and the extracellular media are constant while membrane conductivity depends on TMV as described in Eq. 3. Due to the symmetry of the geometry and to

1   minimize computational time a 2-D axisymmetric model was constructed in COMSOL. Dimensions of

2   simulation space were taken large enough so that electric field in the vicinity of the cell could not be distorted

3   due to boundary conditions. Model parameters are shown in table 1.

4   To model the effect on membrane conductivity of an electroporation pulse in the first microseconds after the

5   onset, the solution of the steady state problem depicted in Fig. 1 represents a proper approximation even though

6   the dynamics of the electroporation phenomena as well as membrane charging process are neglected. At this

7   stage, a few microseconds after the pulse onset, the membrane is completely charged and the very fast increase

8   in membrane conductivity – presumably due to pores – has concluded to be followed by a slow and mild

9   increase during the rest of the pulse (Hibino et al., 1993; Kinosita et al., 1988). the parameters of the model were

10   adjusted to match conductance measurements at 2 μs after the beginning of the pulse from Kinosita and Tsong,

11   (1979), hence it can be assumed that the obtained results will reproduce qualitatively the effect of a pulse within

12   this timescale.

13   The simulated space is about 10^4 times larger than the membrane thickness, which makes the numerical solution

14   complicated and time consuming. To address this, Ivorra et al. (2010) used a membrane thickness 10 times larger

15   than a realistic value (50 nm instead of 5 nm) and rescaled the electrical properties of the membrane to not alter

16   the results. Here, to avoid this complication, each subdomain (extracellular and intracellular) was calculated

17   through a separate application mode of the same type as in (Rems et al., 2013; Retelj et al., 2013), and the

18   membrane was replaced by a surface to which a boundary condition that accounts for membrane conduction and

19   displacement currents (Pucihar et al., 2006, 2009) was added:

$$\vec{n} \cdot \vec{J} = \frac{\sigma_m (V - V_{ref})}{h} + \frac{\varepsilon_m}{h} \frac{\partial (V - V_{ref})}{\partial t} \qquad (5)$$

20

21   where V and V_{ref} are the potentials on the interior and the exterior side of the boundary respectively, ε_m is the

22   permittivity of the membrane, and h is membrane thickness. The product $\vec{n} \cdot \vec{J}$ represents the normal current that

23   flows across the membrane. Note that displacement currents are not taken into account in steady state solutions,

24   thus the second term in Eq. 5 was not included in the computation of steady state solutions.

1
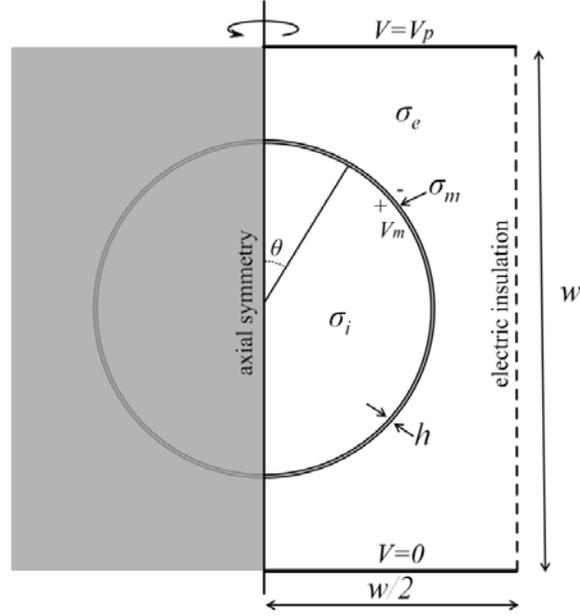
2   **Fig. 1.** Representation of the cell in suspension model implemented for simulation by FEM in COMSOL. Conductivities of

3   the intracellular and extracellular media are constant while membrane conductivity is a function of the local TMV.

Symbol	Value	Definition, justification or source
σ_m	$\sigma_m = \sigma_{m0} + K(e^{\beta|V|} - 1)$	Membrane conductivity(Ivorra et al., 2010)
σ_{m0}	2.5×10^{-7} S/m	Membrane conductivity when TMV=0 if membrane thickness is 5 nm (Gimsa et al., 1996)
β	16	Constant of the conductivity model(Ivorra et al., 2010)
K	$5 \times 10^{-9} \times \sigma_p$	Constant of the conductivity model(Ivorra et al., 2010)
σ_e	1.5 S/m	Extracellular conductivity, isotonic NaCl (Kinosita and Tsong, 1979)
σ_i	0.5 S/m	Intracellular conductivity(Hibino et al., 1993)
σ_p	$(\sigma_e - \sigma_i)/\ln(\sigma_e / \sigma_i)$	Conductivity of the solution inside the pore (Li and Lin, 2010)
h	5 nm	Membrane thickness(Glaser et al., 1988)
w	$10 \times R$	Dimensions of the simulated space (10 times cell radius)

4   **Table 1** Model parameters used in the FEM model with the membrane conductivity model of Ivorra et al. (2010) to calculate
5   the electric potentials and membrane conductivity during an electroporation pulse.

6   According to the model presented in Eqs. 3 and 4, the average membrane conductivity would be related to the

7   area occupied by the pores. Since σ_{m0} and σ_p are constant along the membrane, and the term $\lambda(e^{\beta|TMV|} - 1)$

8   represents the local area occupied by pores at each point of the membrane, the average membrane conductivity is

9   related to the RPA as follows:

$$\overline{\sigma_m} = \sigma_{m0} + \sigma_p \times RPA \tag{6}$$

10   The average conductivity of the membrane, $\overline{\sigma_m}$, was obtained from the COMSOL results post-processor. Then

11   from Eq. 6 it was possible to obtain the RPA. To do so the effective conductivity of the pores was estimated as in

12   (Li and Lin, 2010) :

$$\sigma_p = \frac{\sigma_e - \sigma_i}{\ln(\sigma_e/\sigma_i)} \tag{7}$$

1   Where σ_e and σ_i are the conductivity of the extracellular and the intracellular medium respectively.

2   **Model 2: Pore creation based model**

3   We also performed numerical simulations of the geometry depicted in Fig. 1 using the asymptotic

4   electroporation model from DeBruin and Krassowska (1999). This model states that the pore formation

5   dynamics is governed by the differential equation:

$$\frac{dN}{dt} = \alpha e^{\left(\frac{TMV}{V_{ep}}\right)^2} \left(1 - \frac{N}{N_0} e^{-q\left(\frac{TMV}{V_{ep}}\right)^2} \right) \tag{8}$$

6   where N is the pore density in the membrane, N_0 the equilibrium pore density in the membrane when TMV = 0

7   and parameters α, q and V_{ep} are constants of the model. The creation of pores in the membrane due to the

8   electroporation phenomena causes an increase in membrane conductivity, σ_{ep}, that is calculated as in (Li and

9   Lin, 2010)(Krassowska and Filev, 2007):

$$\sigma_{ep} = N \frac{2\pi r_p^2 \sigma_p h}{\pi r_p + 2h} \tag{9}$$

10 where r_p and h are the radius of the pores and the membrane thickness respectively, and σ_p is the effective

11 conductivity of the solution inside the pores, which was approximated as in the previous section (Eq. 7).

12 To perform numerical simulations, Eq. 8 was included into the model using the *Weak Form Boundary PDE*

13 mode of COMSOL and the problem depicted in Fig.1 was solved in the *Electric currents* mode of the *AC/DC*

14 module of COMSOL (*Time-dependent Study*) using the linear system solver *Pardiso*. As in previous section,

15 membrane was replaced by a surface with a boundary condition (Eq. 5) and the membrane conductivity at each

16 time step was accounted as the sum of the unaltered membrane conductivity σ_{m0} and the conductivity due to

17 electroporation phenomenon σ_{ep} from Eq. 9 ($\sigma_m = \sigma_{m0} + \sigma_{ep}$). Parameters used in the model are shown in

18 Table 2.

Symbol	Value	Definition, justification or source
σ_{m0}	2.5×10^{-7} S/m	Membrane conductivity when TMV=0 if membrane thickness is 5 nm (Gimsa et al., 1996)
σ_e	1.5 S/m	Extracellular conductivity, isotonic NaCl (Kinosita and Tsong, 1979)
σ_i	0.5 S/m	Intracellular conductivity(Hibino et al., 1993)
h	5 nm	Membrane thickness(Glaser et al., 1988)
ε_e	70	Relative permittivity of the extracellular medium (Kotnik and Miklavčič, 2006)
ε_i	70	Relative permittivity of the intracellular medium (Kotnik and Miklavčič, 2006)
ε_m	5	Relative permittivity of the membrane (Kotnik and Miklavčič, 2006)
w	$10 \times R$	Dimensions of the simulated space (10 times cell radius)
σ_p	$(\sigma_e - \sigma_i)/\ln(\sigma_e / \sigma_i)$	Conductivity of the solution inside the pore (Li and Lin, 2010)
σ_m	$\sigma_{m0} + \sigma_{ep}$	Membrane conductivity (see Eq. 9)
r_p	0.76 nm	Pore radius (DeBruin and Krassowska, 1999)
q	2.46	Electroporation constant (DeBruin and Krassowska, 1999)
α	10^9	Electroporation parameter (DeBruin and Krassowska, 1999)
V_{ep}	0.258	Characteristic voltage of electroporation (DeBruin and Krassowska, 1999)
N_0	1.5×10^9 m^{-2}	Equilibrium pore density when TMV=0 (DeBruin and Krassowska, 1999)

Table 2 Model parameters used in the FEM simulations with the electroporation model of DeBruin and Krassowska (1999) to calculate the electric potentials, membrane conductivity and pore density during an electroporation pulse.

To estimate the RPA, first the total number of pores was calculated by integrating the pore density N over the whole membrane surface:

$$N_{tot} = \int N \, dS \qquad (10)$$

Then it was straightforward to obtain the RPA as the quotient between the total surface occupied by pores and the cell surface:

$$RPA = \frac{N_{tot}\pi r_p{}^2}{4\pi R^2} \qquad (11)$$

where R is cell radius.

Transmembrane transport after the pulse

The second criterion used to assess electroporation effectiveness consisted in reaching a certain intracellular concentration of an arbitrary extracellular solute at a long time after the application of the pulse. Since most of the transport takes place after the pulse (Neumann et al., 1998; Puc et al., 2003; Tekle et al., 1990, 1991, 1994); the contribution of both electrophoretic and diffusion transport during the pulse can be neglected. Thus it was only considered the transport by diffusion after the pulse, which can be quantified by Fick's law:

$$\frac{dc(t)}{dt}\frac{V}{S_p(t)} = -D\frac{dc(t)}{dx} \qquad (12)$$

where $c(t)$ is the molar concentration of the considered ion or molecule passing through the surface S_p, which is the effective surface where transport can take place, V is the volume of the cell and D the diffusion constant.

The effective surface of diffusion, $S_p(t)$, in Eq. 12 was defined as the area of the membrane occupied by pores or defects through which ions or molecules can penetrate into the cell. This surface was modeled as time dependent to account for pore resealing.

Several experimental measurements show that resealing occurs in a number of phases. Usually, a sudden decrease in membrane conductivity is observed during the first microseconds or very few milliseconds after the pulse; followed by one or more slower phases (Glaser et al., 1988; Hibino et al., 1993; Neumann et al., 1998). These resealing phases would be linked to permeabilization stages during the preceding electroporation pulse. Recent studies (Demiryurek et al., 2015; Pavlin and Miklavčič, 2008; Pavlin et al., 2007; Silve et al., 2014; Wegner, 2015; Wegner et al., 2011, 2015) suggest that at least two dynamics occur during the pulse that would lead to two different pore populations. First a population of transient or short-lived pores would be created. These pores would take a major role in conductivity increase during the pulse. Second, a given fraction of these

1   short-lived pores would be stabilized forming a population of long-lived pores – or defects in the membrane –

2   through which most of the post-pulse transport would take place.

3   The relationship between the two populations of pores is yet not clear. Experimental results have shown that the

4   fraction of long-lived pores would depend on several parameters such as the electric field, the pulse length and

5   the number of pulses (Pavlin and Miklavčič, 2008; Pavlin et al., 2007). The same studies also showed that under

6   the application of several pulses, while the fraction of short-lived pores would remain the same during each

7   pulse, the fraction of long-lived pores would increase with each consecutive pulse. This increase due to the

8   application of consecutive pulses would also depend on the pulse repetition rate (Silve et al., 2014).

9   Since most of the transport takes place after the pulse, and the hypothetical short-lived pores seem to shrink

10   within a few milliseconds (Benz and Zimmermann, 1981; Glaser et al., 1988; Hibino et al., 1993; Neumann et

11   al., 1998; Pavlin and Miklavčič, 2008; Pavlin et al., 2007), the transport through these pores was neglected in the

12   model employed here. Therefore to approximate the effective diffusion surface, S_p, the focus was on the fraction

13   of the hypothetical long-lived pores and its dynamics. To model this behavior, here it was employed an

14   exponential time decay function:

$$S_p(t) = S_{per} e^{-t/\tau} \qquad (13)$$

15   being S_{per} the surface occupied by the long-lived pores, or defects, at the end of the pulse.

16   Experimental studies on cell membrane permeabilization – based on the influx or efflux of ions and/or molecules

17   – report different timescales for the slow resealing process: hundreds of milliseconds (Lindner et al., 1977;

18   Melikov et al., 2001; Teissié and Tsong, 1981), several seconds (Glaser et al., 1988; Neumann et al., 1998;

19   Pucihar et al., 2008; Rols and Teissié, 1990) and a few minutes (Kinosita and Tsong, 1977; Rols and Teissié,

20   1992; Saulis et al., 1991).

21   The RPA's due to the hypothetical short and long-lived pores have been quantified simultaneously after different

22   number of pulses (Pavlin and Miklavčič, 2008; Pavlin et al., 2007). The percentage of RPA arising from long-

23   lived pores respect to the total RPA ranged from about 5% after a single pulse to about 15% after 8 pulses. Here

24   the value of S_{per} was approximated as a fraction of the surface occupied by pores at the end of the pulse, S_p,

25   taking into account these percentages. That is, the value of the surface occupied by the long-lived pores was

26   computed as the product of the RPA (as obtained in previous sections), the total surface of the cell membrane

27   (S_c) and the fraction of long-lived pores with respect to the total population of pores (f):

$$S_{per} = f \times S_p = f \times RPA \times S_c \qquad (14)$$

1   To find a compact expression for intracellular concentration $c_i(t)$ for long times after the pulse, we need to solve

2   Eq. 12 defining the transport through the membrane surface as the difference between intracellular and

3   extracellular concentration: $c(t) = c_i(t) - c_e(t)$. The following simplifications were made for such purpose:

4   a. For cell suspensions with a low cell volume fraction or for a low final intracellular concentration

5   (compared with the extracellular concentration), the external concentration can be considered constant:

6          $c_e(t) = c_e(0) = c_e$. For instance, for a cell volume fraction of 0.2 and a final intracellular concentration

7   of a 5% the extracellular concentration, the variation in extracellular concentration is less than 2% (see

8   appendix).

9   b. Since ions or molecules considered here cannot enter into the cell in normal conditions and the transport

10   during the pulse can be neglected, the initial intracellular concentration can be approximated to zero:

11         $c_i(0) \approx 0$.

12   c. The term $dc(t)/dx$ is the concentration gradient across the membrane and can be approximated as

13         $(c_i(t) - c_e)/h$, being h cell membrane thickness.

14 After these simplifications, Eq. 12 yields to:

$$c_i(t) = c_e \left(1 - exp \left[\frac{DS_{per}\tau}{Vh} \left(e^{-t/\tau} - 1 \right) \right] \right) \tag{15}$$

15 If it is assumed that the final intracellular concentration is measured a long time after the pulse application, then

16 it is possible to approximate time in Eq. 15 as infinity (practically no transmembrane transport takes place for

17 times longer than a few times the value of τ after the pulse). This leads to a simple expression for the final

18 intracellular concentration after pore resealing:

$$c_i = c_e \left(1 - e^{\frac{-DS_{per}\tau}{Vh}} \right) \tag{16}$$

19 Taking into account how S_{per} was defined, here it was employed the following expression to estimate the RPA

20 during the pulse necessary to reach a certain intracellular concentration from Eq. 16:

$$RPA = ln\left(1 - \frac{c_i}{c_e}\right) \frac{Rh}{3fD\tau} \tag{17}$$

21 where R is cell radius.

22 Imposing values for intracellular and extracellular concentrations (or their ratio), as well as for the diffusion

23 constant and the resealing time constant, this expression (Eq. 17) provides the necessary RPA as function of cell

24 radius. From these values and using the permeabilization models explained in the previous sections it was

25 possible to calculate the necessary applied field as a function of radius in each case by testing different
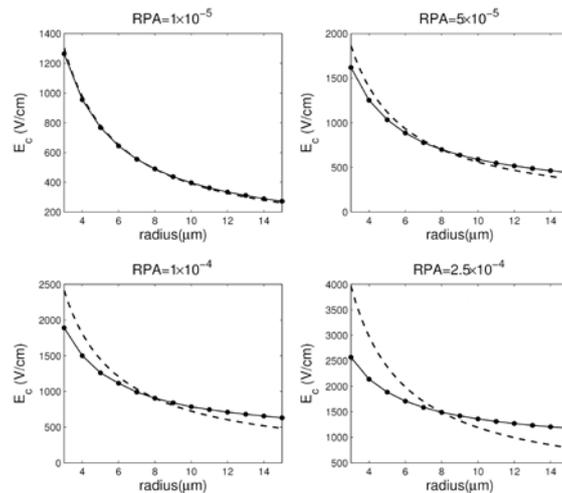
26 magnitudes of the electric field.

1 RESULTS

2 Relative pore area during the pulse

3 The first criterion we defined to assess the necessary applied electric field in order to detect electroporation was

4 to impose a value for the RPA. The values of RPA reported in electroporation experiments range between 10^{-3}

5 and 10^{-5} (Hibino et al., 1991, 1993; Kinosita et al., 1988; Neumann et al., 1998). We simulated the applied

6 electric field required to obtain different values of the RPA at the cell membrane as a function of cell radius.

7 The results obtained with the membrane conductivity model (Ivorra et al., 2010) are depicted in Fig. 2. For a

8 small RPA (1×10^{-5}) the relationship between electric field and cell radius is almost indistinguishable from the

9 *1/r* behavior predicted by Schwan's equation (Eq. 1). However, as we increase the imposed RPA, the electric

10 field dependency on cell radius becomes less steep. Moreover for RPA of 1×10^{-4} and above the simulated

11 results differ significantly from an inverse function of cell radius.

12 Results obtained with the electroporation model based on pore creation (DeBruin and Krassowska, 1999) for a

13 single pulse of 100 μs are shown in Fig. 3. Results are very similar to those obtained using the membrane

14 conductivity model: for a small RPA the results fit with the prediction of a *1/r* relationship between electric field

15 and cell radius; as we impose higher RPA values this dependency becomes less steep, and for RPA values of

16 1×10^{-4} and higher we observe a substantial deviation of simulation results from an inverse dependency on cell

17 radius.

18

Fig. 2. Simulation results according to permeabilization model 1 of the electric field magnitude required to achieve different values of the RPA (relative membrane area occupied by pores) at the end of a 2 μs electroporation pulse (•), compared to a function inversely proportional to the radius and adjusted to the value of the field at 8 μm (dashed line). Simulated results are based on the model geometry depicted in Fig. 1 and the membrane conductivity model presented in the Materials and Methods section. The RPA was evaluated according to Eq. 6.
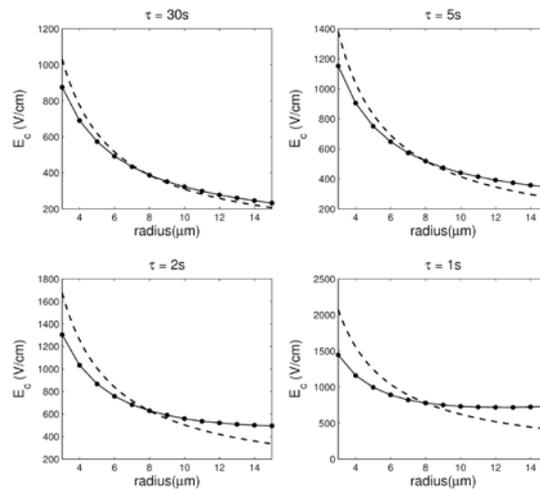
Final intracellular concentration

The other criterion we defined for assessing effective electroporation was based on imposing the minimum final intracellular concentration after the pulse for a given molecule.

Besides defining a value for the final intracellular concentration, we needed to choose plausible values for the diffusion constant (see Eq. 16), as well as the fraction of long-lived pores respect to the total (see Eq. 14). The diffusion constants for dyes and molecules typically used in electroporation experiments reported in the literature are in the range from 10^{-9} to 10^{-10} $m^2 \cdot s^{-1}$ (Gendron et al., 2008; Neumann et al., 1998; Petrášek and Schwille, 2008; Renkin, 1954). Regarding the value of the fraction of long lived-pores, we used the value measured experimentally after a single pulse of 100 μs (Pavlin and Miklavčič, 2008) that was a 5%. Then to obtain the results displayed in Fig. 4 and Fig. 5 we imposed a final intracellular concentration value of 5% of the initial extracellular concentration, a value of 2×10^{-10} $m^2 \cdot s^{-1}$ for the diffusion constant D – which is the value measured experimentally for the propidium iodide (Jimenez et al., 2014) – and different values of the resealing time constant τ.

The results obtained by combining the diffusion model and the membrane conductivity model are displayed in Fig. 4. When τ is decreased, the dependency of the electric field on cell radius becomes less steep and simulation results deviate from the expected inverse relationship between radius and electric field. For a $\tau = 2$ seconds a plateau is observed above $R = 8$ μm where there is no dependence of electric field on cell radius and for $\tau = 1$ second the dependence is very weak for all simulated values of cell radius.

1   Fig. 5 shows the results obtained by combining the diffusion model and the electroporation model based on pore

2   creation. Results are very similar to those obtained with the membrane conductivity model although we needed

3   to define lower values of τ to observe a significant deviation from the expected inverse relationship between

4   radius and electric field. In this case results with $\tau = 1$ second show a plateau for radius above $R = 8$ μm and

5   results obtained for $\tau = 0.5$ seconds exhibit a very weak dependence on cell radius.

6
7   **Fig. 4.** Simulation results of the electric field magnitude required to achieve a final intracellular concentration value of a 5%
8   the extracellular concentration for different values of the resealing time constant τ (•),compared to a function inversely
9   proportional to the radius and adjusted to the value of the field at 8 μm (dashed line). These results were obtained combining
10   the diffusion model presented in the previous section and the permeabilization model 1.
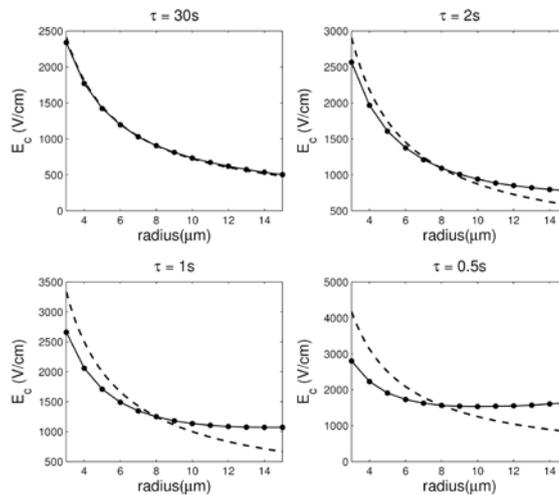
11
12   **Fig. 5** Simulation results of the electric field magnitude required to achieve a final intracellular concentration value of a 5%
13   the extracellular concentration for different values of the resealing time constant τ (•),compared to a function inversely
14   proportional to the radius and adjusted to the value of the field at 8 μm (dashed line). Results were obtained combining the
15   diffusion model presented in the previous section and the permeabilization model 2.

DISCUSSION

Relative pore area during the pulse

We calculated the electric field necessary to achieve a RPA as a function of cell radius with two different permeabilization models: a membrane conductivity model based on experimental measurements, and an electroporation model based on the creation of pores. Both models provided similar results indicating that as the imposed RPA is increased the dependency of the electric field on cell radius becomes less steep.

The results obtained with this first criterion can be intuitively explained: since an increase of the RPA means a membrane conductivity increase, as we get to higher values of the RPA we move away from the condition of a nearly insulating membrane that is assumed in the derivation of Schwan's equation. In particular, due to the short-circuiting effect (explained in the introduction), the local TMV in those regions of the cell that are already electroporated cannot increase substantially by increasing the external field. This means that above a certain value of the electric field the regions of the membrane that are easier to permeabilize (poles facing the electrodes) will not experience a substantial raise of its local conductivity. Thus in these cases the average conductivity increase for larger fields will be due to an increase in the local conductivity of the regions far from the poles facing the electrodes. This is related to the flattening observed in the TMV profiles for electric fields above a certain value, and it means that an increase in the RPA can only be accomplished by permeabilizing a larger area of the cell membrane and not so much by further permeabilizing the areas that are already permeabilized. Therefore the deviation between the expected dependence of electric field on cell radius and simulation results gets more pronounced as we increase the value of the RPA.

Final intracellular concentration

We calculated the electric field required to reach a certain intracellular concentration as a function of cell radius. The results indicate that depending on the resealing dynamics the dependency of the critical electric field on cell radius can either deviate from the expected $1/r$ relationship according to Schwan's equation model or show a dependency very close to that expected. Results similar to those displayed in Fig. 4 and Fig. 5 can be obtained by imposing different values of the final intracellular concentration and adjusting the values of τ or D. Decreasing τ means that there is less time for the transmembrane transport to take place, and decreasing D means that it is more difficult for the ions or molecules to penetrate into the cell, respectively. Thus lowering one of these two values implies that the initial diffusion surface must be larger in order to reach the same concentration values. Since the diffusion surface is proportional to the RPA, to increase this surface, membrane conductivity during

1   the pulse has to reach values that are far from the assumption of a nearly insulating membrane in Schwan's

2   equation. On the other hand increasing either τ or D makes transport easier. This means that lower RPA values

3   are required to reach the same concentration, and, as we saw previously for low RPA values, the dependence of

4   the field magnitude on cell radius is similar to the *1/r* behavior.

5   From Eq. 17 we can see that for a given D and τ, larger cells require larger values of the RPA to reach a given

6   intracellular concentration. This, in comparison to the assessment based on setting a specific RPA during the

7   pulse, leads to a larger deviation between the Schwan's equation model and the simulated dependence of the

8   critical electric field on cell radius.

9   In the following paragraphs we will discuss some methodological aspects that require further clarification as well

10   as the limitations of this study.

11   In the derivation of Eq. 16 it was assumed that transport during the pulse could be neglected. To validate this

12   assumption, transport during the pulse was quantified as in (Pucihar et al., 2008). The results (not reported here)

13   indicate that the contribution of the transport during the pulse on intracellular concentration is at least five orders

14   of magnitude lower than final concentration even for pulses in the millisecond range. Hence, we conclude that

15   for this analysis transport during the pulse can be ignored, and that this simplification has no impact on the

16   conclusions of the present study.

17   Regarding the criterion of imposing a final intracellular concentration, it must be noted that, cell electroporation

18   assessment and the detection limit depends substantially on the molecules used and on the detection method

19   (Gabriel and Teissié, 1999; He et al., 2007; Pucihar et al., 2008). For instance a cytotoxic agent such as

20   bleomycin as few as 500 molecules are needed to kill the cell by a mitotic cell death process (Poddevin et al.,

21   1991; Silve and Mir, 2011; Tounekti et al., 1993). On the other hand, when using fluorescence imaging to detect

22   the uptake of a given dye such as propidium iodide, a significant concentration of this dye is needed, at least

23   locally, to be able to distinguish the fluorescence signal from noise. In a real experiment the detection does not

24   depend on the average concentration but in the local concentration, in fact generally fluorescence images present

25   an accumulation in the regions close to the membrane in the areas facing the electrodes. Nevertheless we used a

26   simplified criterion – the average concentration – and an arbitrary value, since the aim was to study how the

27   transmembrane transport can vary depending on the electric field, the cell radius, the diffusion constant and the

28   pore lifetime.

29   To estimate the effective diffusion surface we used an experimental value that relates the total surface of the

30   whole population of membrane defects (presumably pores) with the surface occupied by long-lived membrane

defects. As explained in the Materials and Methods section, the relation between the long-lived population and the whole population of pores is yet not clear, however, experiments suggest that it depends on the electric field, pulse length, the number of pulses and the pulse repetition rate.

In this study only a single pulse was considered for computing both membrane permeabilization and transmembrane transport. This neglects the fact that, commonly, an electroporation treatment consists in a train of several pulses since it has been observed that multiple pulses are more effective than a single pulse. Nevertheless, it must be noted that the experimental discrepancies regarding the electric field threshold to detect electroporation and its dependency on cell radius were found also for measurements with single pulse protocols (Agarwal et al., 2007; Henslee et al., 2011; Hojo et al., 2003; Towhidi et al., 2008). Therefore, we considered adequate to model a single pulse treatment for the sake of simplicity. Furthermore, it must be noted that mechanisms acting in the electroporation phenomenon that cause the influence of the number of pulses and its repetition rate are yet not elucidated and that the quantification of these effects cannot be accurately modeled. A recent model (Leguèbe et al., 2014) describes separately the conductivity increase during the pulse and the long term permeabilization of the cell membranes. That model proved to be able to reproduce qualitatively the experimental observations on the uptake of propidium iodide and the dependency of this uptake on the pulse repetition rate. Nevertheless the parameters of the model need to be calibrated to describe quantitatively the phenomenon and the sensitivity of the model to these parameters would have to be investigated before considering its use in our study.

CONCLUSIONS

The motivation of the present study was to explore a plausible explanation to the apparently contradictory results that can be found in the electroporation literature regarding the electric field threshold dependency on the cell radius. In particular, it has been attempted to find an explanation to those experimental results that do not follow the Schwan's equation model in which the threshold is predicted to be inversely proportional to the cell radius.

While the Schwan's equation model describes when electroporation can be initiated, its relation to detectable outcomes of electroporation (e.g. dye uptake) is more indirect. We therefore hypothesized that by modeling the effects of electroporation, we would be able to predict results not compatible with the Schwan's equation model under some circumstances. And, indeed we have shown that by modeling the interplay between cell membrane conductivity, permeability and transmembrane voltage we obtain electric field thresholds for detection of electroporation that depart from the Schwan's equation model. Departure from the Schwan's equation model is

particularly significant when it is imposed that cell membrane permeabilization has to reach a high value during the pulse (RPA > 10^{-4}) whereas it is almost unnoticeable when the imposed permeabilization is low (RPA < 10^{-5}). When uptake of an extracellular molecule is modeled, departure from the Schwan's equation model is even further exaggerated. These results have been obtained using two different electroporation models.

APPENDIX

Variation in extracellular concentration

Assuming that the initial intracellular concentration is zero and there is no change in cell volume during the experiments, initial and final concentrations can be written as:

$$\begin{cases} c_{i,0} = 0 \\ c_{e,0} = N_0/V(1-F) \\ c_{i,f} = N/F \times V \\ c_{e,f} = (N_0 - N)/V(1-F) \end{cases} \tag{A.1}$$

being N_0 the total number of molecules, N the number of molecules that enter the cell, V the total volume of the suspension and F the cell volume fraction. If we express the final intracellular concentration as a fraction of the initial extracellular concentration $c_{i,f} = a \times c_{e,i}$, then from (A.1):

$$a = \frac{c_{i,f}}{c_{e,i}} = \frac{N(1-F)}{N_0 F} \tag{A.2}$$

On the other hand, from (A.1), the relationship between final and initial extracellular concentration is:

$$\frac{c_{e,f}}{c_{e,0}} = \frac{N_0 - N}{N_0} \tag{A.3}$$

Combining A.2 and A.3 we can obtain an expression of the term $c_{e,f}/c_{e,0}$ as a function of F and a:

$$\frac{c_{e,f}}{c_{e,0}} = \frac{1 - F(1+a)}{1-F} \tag{A.4}$$

For a cell volume fraction of 0.2 and a final intracellular concentration of 5% the initial extracellular concentration, the variation of the extracellular concentration is 1.25%.

REFERENCES

Abiror, I.G., Arakelyan, V.B., Chernomordik, L.V., Chizmadzhev, Y.A., Pastushenko, V.F., and Tarasevich, M.R. (1979). 246 - Electric breakdown of bilayer lipid membranes I. The main experimental facts and their qualitative discussion. Bioelectrochemistry Bioenerg. *6*, 37–52.

Agarwal, A., Zudans, I., Weber, E.A., Olofsson, J., Orwar, O., and Weber, S.G. (2007). Effect of Cell

1   Size and Shape on Single-Cell Electroporation. Anal. Chem. *79*, 3589–3596.

2   Benz, R., and Zimmermann, U. (1980). 376 - Relaxation studies on cell membranes and lipid bilayers

3   in the high electric field range. Bioelectrochemistry Bioenerg. *7*, 723–739.

4   Benz, R., and Zimmermann, U. (1981). The resealing process of lipid bilayers after reversible

5   electrical breakdown. Biochim. Biophys. Acta (BBA)- … *640*, 169–178.

6   Ĉemazâr, M., Jarm, T., Miklavĉiĉ, D., Lebar, A.M., Ihan, A., Kopitar, N.A., and Serŝa, G. (1998).

7   Effect of Electric-Field Intensity on Electropermeabilization and Electrosensitmty of Various Tumor-

8   Cell Lines In Vitro. Electro- and Magnetobiology *17*, 263–272.

9   Chen, C., Smye, S.W., Robinson, M.P., and Evans, J. a. (2006). Membrane electroporation theories: A

10   review. Med. Biol. Eng. Comput. *44*, 5–14.

11   DeBruin, K. a, and Krassowska, W. (1999). Modeling electroporation in a single cell. I. Effects Of

12   field strength and rest potential. Biophys. J. *77*, 1213–1224.

13   Delemotte, L., and Tarek, M. (2012). Molecular Dynamics Simulations of Lipid Membrane

14   Electroporation. J. Membr. Biol. *245*, 531–543.

15   Demiryurek, Y., Nickaeen, M., Zheng, M., Yu, M., Zahn, J.D., Shreiber, D.I., Lin, H., and Shan, J.W.

16   (2015). Transport, resealing, and re-poration dynamics of two-pulse electroporation-mediated

17   molecular delivery. Biochim. Biophys. Acta - Biomembr. *1848*, 1706–1714.

18   Djuzenova, C.S., Sukhorukov, V.L., Klöck, G., Arnold, W.M., and Zimmermann, U. (1994). Effect of

19   electric field pulses on the viability and on the membrane-bound immunoglobulins of LPS-activated

20   murine B-lymphocytes: correlation with the cell cycle. Cytometry *15*, 35–45.

21   Frey, W., White, J.A., Price, R.O., Blackmore, P.F., Joshi, R.P., Nuccitelli, R., Beebe, S.J.,

22   Schoenbach, K.H., and Kolb, J.F. (2006). Plasma Membrane Voltage Changes during Nanosecond

23   Pulsed Electric Field Exposure. Biophys. J. *90*, 3608–3615.

24   Gabriel, B., and Teissié, J. (1999). Time Courses of Mammalian Cell Electropermeabilization

25   Observed by Millisecond Imaging of Membrane Property Changes during the Pulse. Biophys. J. *76*,

26   2158–2165.

27   Gendron, P.-O., Avaltroni, F., and Wilkinson, K.J. (2008). Diffusion Coefficients of Several

28   Rhodamine Derivatives as Determined by Pulsed Field Gradient–Nuclear Magnetic Resonance and

Fluorescence Correlation Spectroscopy. J. Fluoresc. *18*, 1093–1101.

Gimsa, J., Müller, T., Schnelle, T., and Fuhr, G. (1996). Dielectric spectroscopy of single human erythrocytes at physiological ionic strength: dispersion of the cytoplasm. Biophys. J. *71*, 495–506.

Glaser, R.W., Leikin, S.L., Chernomordik, L. V, Pastushenko, V.F., and Sokirko, A.I. (1988). Reversible electrical breakdown of lipid bilayers: Formation and Evolution of Pores. Biochim. Biophys. Acta *940*, 275–287.

Golzio, M., Teissié, J., and Rols, M.-P. (2002). Cell synchronization effect on mammalian cell permeabilization and gene delivery by electric field. Biochim. Biophys. Acta - Biomembr. *1563*, 23–28.

He, H., Chang, D.C., and Lee, Y.K. (2007). Using a micro electroporation chip to determine the optimal physical parameters in the uptake of biomolecules in HeLa cells. Bioelectrochemistry *70*, 363–368.

Henslee, B.E., Morss, A., Hu, X., Lafyatis, G.P., and Lee, L.J. (2011). Electroporation dependence on cell size: Optical tweezers study. Anal. Chem. *83*, 3998–4003.

Hibino, M., Shigemori, M., Itoh, H., Nagayama, K., and Kinosita, K. (1991). Membrane conductance of an electroporated cell analyzed by submicrosecond imaging of transmembrane potential. Biophys. J. *59*, 209–220.

Hibino, M., Itoh, H., and Kinosita, K. (1993). Time courses of cell electroporation as revealed by submicrosecond imaging of transmembrane potential. Biophys. J. *64*, 1789–1800.

Ho, M.-C., Casciola, M., Levine, Z.A., and Vernier, P.T. (2013). Molecular dynamics simulations of ion conductance in field-stabilized nanoscale lipid electropores. J. Phys. Chem. B *117*, 11633–11640.

Hojo, S., Shimizu, K., Yositake, H., Muraji, M., Tsujimoto, H., and Tatebe, W. (2003). The relationship between electropermeabilization and cell cycle and cell size of Saccharomyces cerevisiae. IEEE Trans. Nanobioscience *2*, 35–39.

Ibey, B.L., Roth, C.C., Pakhomov, A.G., Bernhard, J. a., Wilmink, G.J., and Pakhomova, O.N. (2011). Dose-Dependent Thresholds of 10-ns Electric Pulse Induced Plasma Membrane Disruption and Cytotoxicity in Multiple Cell Lines. PLoS One *6*, e15642.

Ivorra, A., and Rubinsky, B. (2007). In vivo electrical impedance measurements during and after

electroporation of rat liver. Bioelectrochemistry *70*, 287–295.

Ivorra, A., Villemejane, J., and Mir, L.M. (2010). Electrical modeling of the influence of medium

conductivity on electroporation. Phys. Chem. Chem. Phys. *12*, 10055–10064.

Jimenez, A.J., Maiuri, P., Lafaurie-Janvore, J., Divoux, S., Piel, M., and Perez, F. (2014). ESCRT

Machinery Is Required for Plasma Membrane Repair. Science (80-.). *343*, 1247136–1247136.

Kinosita, K., and Tsong, T.Y. (1979). Voltage-induced conductance in human erythrocyte membranes.

Biochim. Biophys. Acta - Biomembr. *554*, 479–497.

Kinosita, K.J., and Tsong, T.Y. (1977). Formation and resealing of pores of controlled sizes in human

erythrocyte membrane. Nature *268*, 438–441.

Kinosita, K., Ashikawa, I., Saita, N., Yoshimura, H., Itoh, H., Nagayama, K., and Ikegami, A. (1988).

Electroporation of cell membrane visualized under a pulsed-laser fluorescence microscope. Biophys. J.

53, 1015–1019.

Kotnik, T., and Miklavcic, D. (2000). Analytical description of transmembrane voltage induced by

electric fields on spheroidal cells. Biophys. J. *79*, 670–679.

Kotnik, T., and Miklavčič, D. (2006). Theoretical Evaluation of Voltage Inducement on Internal

Membranes of Biological Cells Exposed to Electric Fields. Biophys. J. *90*, 480–491.

Krassowska, W., and Filev, P.D. (2007). Modeling electroporation in a single cell. Biophys. J. *92*,

404–417.

Leguèbe, M., Silve, A., Mir, L.M., and Poignard, C. (2014). Conducting and permeable states of cell

membrane submitted to high voltage pulses: Mathematical and numerical studies validated by the

experiments. J. Theor. Biol. *360*, 83–94.

Li, J., and Lin, H. (2010). The current-voltage relation for electropores with conductivity gradients.

Biomicrofluidics *4*, 1–17.

Lindner, P., Neumann, E., and Rosenheck, K. (1977). Kinetics of permeability changes induced by

electric impulses in chromaffin granules. J Membr Biol *32*, 231–254.

Mauroy, C., Portet, T., Winterhalder, M., Bellard, E., Blache, M.C., Teissié, J., Zumbusch, A., and

Rols, M.P. (2012). Giant lipid vesicles under electric field pulses assessed by non invasive imaging.

Bioelectrochemistry *87*, 253–259.

1 Melikov, K.C., Frolov, V.A., Shcherbakov, A., Samsonov, A. V, Chizmadzhev, Y.A., and

2 Chernomordik, L. V (2001). Voltage-induced nonconductive pre-pores and metastable single pores in

3 unmodified planar lipid bilayer. Biophys. J. *80*, 1829–1836.

4 Neumann, E., Toensing, K., Kakorin, S., Budde, P., and Frey, J. (1998). Mechanism of electroporative

5 dye uptake by mouse B cells. Biophys. J. *74*, 98–108.

6 Pakhomov, A.G., Kolb, J.F., White, J. a., Joshi, R.P., Xiao, S., and Schoenbach, K.H. (2007). Long-

7 lasting plasma membrane permeabilization in mammalian cells by nanosecond Pulsed Electric Field

8 (nsPEF). Bioelectromagnetics *28*, 655–663.

9 Pavlin, M., and Miklavčič, D. (2008). Theoretical and experimental analysis of conductivity, ion

10 diffusion and molecular transport during cell electroporation — Relation between short-lived and

11 long-lived pores. Bioelectrochemistry *74*, 38–46.

12 Pavlin, M., Kanduser, M., Rebersek, M., Pucihar, G., Hart, F.X., Magjarevic, R., and Miklavcic, D.

13 (2005). Effect of cell electroporation on the conductivity of a cell suspension. Biophys J *88*, 4378–

14 4390.

15 Pavlin, M., Leben, V., and Miklavčič, D. (2007). Electroporation in dense cell suspension—

16 Theoretical and experimental analysis of ion diffusion and cell permeabilization. Biochim. Biophys.

17 Acta - Gen. Subj. *1770*, 12–23.

18 Petrášek, Z., and Schwille, P. (2008). Precise Measurement of Diffusion Coefficients using Scanning

19 Fluorescence Correlation Spectroscopy. Biophys. J. *94*, 1437–1448.

20 Poddevin, B., Orlowski, S., Belehradek, J., and Mir, L.M. (1991). Very high cytotoxicity of bleomycin

21 introduced into the cytosol of cells in culture. Biochem. Pharmacol. *42*, S67–S75.

22 Puc, M., Kotnik, T., Mir, L.M., and Miklavčič, D. (2003). Quantitative model of small molecules

23 uptake after in vitro cell electropermeabilization. Bioelectrochemistry *60*, 1–10.

24 Pucihar, G., Kotnik, T., Valič, B., and Miklavčič, D. (2006). Numerical determination of

25 transmembrane voltage induced on irregularly shaped cells. Ann. Biomed. Eng. *34*, 642–652.

26 Pucihar, G., Kotnik, T., Miklavčič, D., and Teissié, J. (2008). Kinetics of Transmembrane Transport of

27 Small Molecules into Electropermeabilized Cells. Biophys. J. *95*, 2837–2848.

28 Pucihar, G., Miklavčič, D., and Kotnik, T. (2009). A time-dependent numerical model of

transmembrane voltage inducement and electroporation of irregularly shaped cells. IEEE Trans.

Biomed. Eng. *56*, 1491–1501.

Rems, L., Ušaj, M., Kandušer, M., Reberšek, M., Miklavčič, D., and Pucihar, G. (2013). Cell

electrofusion using nanosecond electric pulses. Sci. Rep. *3*, 3382.

Renkin, E.M. (1954). Filtration, diffusion, and molecular sieving through porous cellulose membranes.

J. Gen. Physiol. *38*, 225–243.

Retelj, L., Pucihar, G., and Miklavcic, D. (2013). Electroporation of Intracellular Liposomes Using

Nanosecond Electric Pulses&amp – A Theoretical Study. IEEE Trans. Biomed. Eng. *60*, 2624–2635.

Rols, M.P., and Teissié, J. (1990). Electropermeabilization of mammalian cells. Quantitative analysis

of the phenomenon. Biophys. J. *58*, 1089–1098.

Rols, M.-P., and Teissié, J. (1992). Experimental evidence for the involvement of the cytoskeleton in

mammalian cell electropermeabilization. Biochim. Biophys. Acta *1111*, 45–50.

Sale, a. J.H., and Hamilton, W. a. (1968). Effects of high electric fields on micro-organisms III. Lysis

of erytrhocytes and protoplasts. Biochim. Biophys. Acta - Biomembr. *163*, 37–43.

Saulis, G., Venslauskas, M.S., and Naktinis, J. (1991). Kinetics of pore resealing in cell membranes

after electroporation. J. Electroanal. Chem. Interfacial Electrochem. *321*, 1–13.

Silve, A., and Mir, L.M. (2011). Cell Electropermeabilization and Cellular Uptake of Small

Molecules: The Electrochemotherapy Concept. In Clinical Aspects of Electroporation, T.S. Kee, J.

Gehl, and W.E. Lee, eds. (New York, NY: Springer New York), pp. 69–82.

Silve, a, Guimerà Brunet, a, Al-Sakere, B., Ivorra, a, and Mir, L.M. (2014). Comparison of the

effects of the repetition rate between microsecond and nanosecond pulses: electropermeabilization-

induced electro-desensitization? Biochim. Biophys. Acta *1840*, 2139–2151.

Sixou, S., and Teissié, J. (1990). Specific electropermeabilization of leucocytes in a blood sample and

application to large volumes of cells. Biochim. Biophys. Acta - Biomembr. *1028*, 154–160.

Tarek, M. (2005). Membrane Electroporation: A Molecular Dynamics Simulation. Biophys. J. *88*,

4045–4053.

Teissié, J., and Rols, M.P. (1993). An experimental evaluation of the critical potential difference

inducing cell membrane electropermeabilization. Biophys. J. *65*, 409–413.

1   Teissié, J., and Tsong, T.Y. (1981). Electric field induced transient pores in phospholipid bilayer

2   vesicles. Biochemistry *20*, 1548–1554.

3   Tekle, E., Astumian, R.D., and Chock, P.B. (1990). Electro-permeabilization of cell membranes:

4   Effect of the resting membrane potential. Biochem. Biophys. Res. Commun. *172*, 282–287.

5   Tekle, E., Astumian, R.D., and Chock, P.B. (1991). Electroporation by using bipolar oscillating

6   electric field: an improved method for DNA transfection of NIH 3T3 cells. Proc. Natl. Acad. Sci. U. S.

7   A. *88*, 4230–4234.

8   Tekle, E., Astumian, R.D., and Chock, P.B. (1994). Selective and asymmetric molecular transport

9   across electroporated cell membranes. Proc. Natl. Acad. Sci. U. S. A. *91*, 11512–11516.

10   Tekle, E., Astumian, R.D., Friauf, W.A., and Chock, P.B. (2001). Asymmetric Pore Distribution and

11   Loss of Membrane Lipid in Electroporated DOPC Vesicles. Biophys. J. *81*, 960–968.

12   Tounekti, O., Pron, G., Belehradek, J., and Mir, L.M. (1993). Bleomycin, an apoptosis-mimetic drug

13   that induces two types of cell death depending on the number of molecules internalized. Cancer Res.

14   *53*, 5462–5469.

15   Towhidi, L., Kotnik, T., Pucihar, G., Firoozabadi, S.M.P., Mozdarani, H., and Miklavčič, D. (2008).

16   Variability of the Minimal Transmembrane Voltage Resulting in Detectable Membrane

17   Electroporation. Electromagn. Biol. Med. *27*, 372–385.

18   Vernier, P.T., Ziegler, M.J., Sun, Y., Gundersen, M.A., and Tieleman, D.P. (2006). Nanopore-

19   facilitated, voltage-driven phosphatidylserine translocation in lipid bilayers—in cells and in silico.

20   Phys. Biol. *3*, 233–247.

21   Wegner, L.H. (2015). The conductance of cellular membranes at supra-physiological voltages.

22   Bioelectrochemistry *103*, 34–38.

23   Wegner, L.H., Flickinger, B., Eing, C., Berghöfer, T., Hohenberger, P., Frey, W., and Nick, P. (2011).

24   A patch clamp study on the electro-permeabilization of higher plant cells: Supra-physiological

25   voltages induce a high-conductance, K+ selective state of the plasma membrane. Biochim. Biophys.

26   Acta - Biomembr. *1808*, 1728–1736.

27   Wegner, L.H., Frey, W., and Silve, A. (2015). Electroporation of DC-3F cells is a dual process.

28   Biophys. J. *108*, 1660–1671.

1 White, J.A., Pliquett, U., Blackmore, P.F., Joshi, R.P., Schoenbach, K.H., and Kolb, J.F. (2011).

2 Plasma membrane charging of Jurkat cells by nanosecond pulsed electric fields. Eur. Biophys. J. *40*,

3 947–957.

4 Ziegler, M.J., and Vernier, P.T. (2008). Interface Water Dynamics and Porating Electric Fields for

5 Phospholipid Bilayers. J. Phys. Chem. B *112*, 13588–13596.

6 Zimmermann, U., Pilwat, G., and Riemann, F. (1974). Dielectric Breakdown of Cell Membranes.

7 Biophys. J. *14*, 881–899.

8